# Impacts of Hurricane Irma (2017) on ocean transport processes

Thomas Dobbelaere[a,*], Milan Curcic[b], Matthieu le Hénaff[c,d], Emmanuel Hanert[a,e]

[a] *Eath and Life Institute (ELI), UCLouvain, Louvain-la-Neuve, Belgium*
[b] *Rosenstiel School of Marine and Atmospheric Sciences (RSMAS), University of Miami, Coral Gables, Florida, USA*
[c] *Cooperative Institute for Marine and Atmospheric Studies (CIMAS), University of Miami, Miami, Florida, USA*
[d] *Atlantic Oceanographic and Meteorological Laboratory (AOML), NOAA, Miami, Florida, USA*
[e] *Institute of Mechanics, Materials and Civil Engineering (IMMC), UCLouvain, Louvain-la-Neuve, Belgium*

**Abstract**

Tropical cyclones are becoming more intense and more frequent. Their effect is particularly acute in coastal areas where they cause extensive damage leading to an influx of debris, sediments and waste to the sea. However, most coastal ocean models do not represent their transport correctly as they do not couple the hydrodynamics with the wind-generated waves. This may lead to significant errors in heavy-wind conditions. Here, we investigate current-wave interactions during a major cyclone and assess their impact on transport processes. We do that by coupling the unstructured-mesh coastal ocean model SLIM with the spectral wave model SWAN, and applying it to the Florida Reef Tract during Hurricane Irma (Sept. 17). We show that the coupled model successfully reproduces the wave behavior, the storm surge and the ocean currents during the passage of the hurricane. We then use the coupled and uncoupled wave-current model to simulate the transport of

*Corresponding author
*Email address:* `thomas.dobbelaere@uclouvain.be` (Thomas Dobbelaere)

passive drifters. We show that the wave force alone can lead to changes of up to 1 m/s in the modelled currents, which in turn leads to differences of up to 10 km in the position of drifting material over the duration of the hurricane. [Add a sentence on Stokes drift vs wave-current coupling]. Our results suggest that wave-current interactions can strongly impact the transport of drifting material such as sediments and debris in the aftermath of a hurricane. They should thus be taken into account in order to correctly assess its overall impact

*Keywords:*

---

## 1. Introduction

Tropical cyclones are becoming more intense and more frequent (Bhatia et al., 2019; Kossin et al., 2020). This increase is likely due to climate change and will probably continue in the future (Knutson et al., 2020). However, estimating the impact of tropical cyclones on the coastal ocean circulation remains a challenge. Understanding wave-current interactions and being able to represent their impact on coastal ocean transport processes is central to many coastal activities such as dredging, erosion management, O&G, search and rescue (Bever and MacWilliams, 2013; Li and Johns, 1998; Breivik et al., 2013). It would for instance allow to predict hurricane impacts in events such such as the Deepwater Horizon oil spill in the Gulf of Mexico in 2010 (Le Hénaff et al., 2012).

Wave-current interactions during a cyclone are highly nonlinear and can vary significantly in space and time (Wu et al., 2011). Wave-induced currents are generated by wave radiation stress gradients (Longuet-Higgins, 1970), affecting water levels near shorelines and wave breaking points (Longuet-Higgins and Stewart, 1964). Changes in water levels and currents, in turn, affect the motion and evolution of the waves (Sikirić et al., 2013). Coupled wave-current models are therefore required to capture these complex interactions. In order to accurately include surface waves in their equations, such models require the computation of the the full two-dimensional wave spectrum (Van Den Bremer and Breivik, 2018). Spectral wave model are therefore needed.

Coastal oceans are characterized by the complex topography of the coastline and the presence of islands, reefs and artificial structures. Traditional structured-grid models often lack the flexibility to simulate near-shore processes at a sufficiently small scale. Instead, unstructured-mesh models can easily adapt to the topography and are hence better suited to coastal processes (Wu et al., 2011; Chen et al., 2007). Being able to capture the impact of the topography on wave interactions becomes even more important in the case of tropical cyclones. Heavy winds generate large wind-waves and disturb ocean conditions (Liu et al., 2020) by causing coastal upwellings on continental shelves (Smith, 1982) and inducing strong currents, waves and storm surges in nearshore and coastal regions (Dietrich et al., 2010; Weisberg and Zheng, 2006).

The transport of drifting objects or substances that are locally released is often best represented by a Lagrangian individual-based model. Such an approach is routinely used to model the dispersal of larvae, pollutants, sediments and many other tracers (e.g. Le Hénaff et al. (2012); Liubartseva et al. (2018); Figueiredo et al. (2013); Frys et al. (2020)). Although some transport models take the impact of waves into account by adding a Stokes drift velocity, *i.e.* the net drift of a floating particle in the direction of the wave propagation (Van Den Bremer and Breivik, 2018), to the Eulerian currents, they usually neglect the wave-induced currents. Such practice is reasonable in the case of fair weather, when wave-induced forces exerted on currents are relatively small, but might lead to significant errors during storm conditions (Röhrs et al., 2012; Curcic et al., 2016).

The objective of this study is therefore to assess the importance of wave-current interactions during a tropical cyclone. We investigate the transport of drifting particles on the Florida shelf during Hurricane Irma, one of the strongest and costliest tropical cyclones on record in the Atlantic Basin (Xian et al., 2018), which made landfall in Florida in September 2017. To do that, we developed an unstructured coupled wave-current model of South Florida to simulate the ocean circulation during hurricane Irma. Both modelled currents and waves were validated against field measurements and were then used to simulate the transport of drifting material in the Florida Keys and the Florida inner shelf. Model outputs were then compared with uncoupled simulation results in order to assess the impact of wave-induced forces and Stokes drift on the modelled currents and transports.

## 2. Methods

### *2.1. Study area and observational data*

The large-scale ocean circulation around South Florida is dominated by the Florida Current (FC), which originates from the Loop Current (LC) where it enters the Florida Straits from the Gulf of Mexico, and, downstream, forms the Gulf Stream. The FC is a major western boundary current characterized by spatial variability and meandering, associated with the presence of cyclonic eddies between the core of the current and the complex reef topography of the Florida Reef Tract (FRT) (Lee et al., 1995; Kourafalou and Kang, 2012). The variability of the FC extends over a large range of spatial and temporal scales, with periods of 30-70 days in the Lower Keys (Lee et al., 1995) and shorter periods of 2-21 days in the Upper Keys (Lee and Mayer, 1977), and exhibits significant seasonal and interannual cycles (Johns and Schott, 1987; Lee and Williams, 1988; Schott et al., 1988). Circulation on the West Florida Shelf (WFS) on the other hand is forced by local winds and tidal fluctuations (Lee and Smith, 2002; Liu and Weisberg, 2012). Furthermore, due to its location relative to the warm waters of the North Atlantic, Florida is particularly vulnerable to tropical cyclones. On average, the state gets hit by a hurricane every two years and strong hurricanes, some of which the most destructive on record, strike Florida on average once every four years. Malmstadt et al. (2009).

The state of the ocean around Florida is monitored by an extensive array of tide gauges, current meters and buoys. In this study, we used sea surface elevation measurements from the National Oceanic and Atmospheric Administrations (NOAA) Tides and Currents dataset. These measurements were taken at four locations: two in the Florida Keys (Key West and Vaca Key); one on the eastern coast of Florida (Virginia Key); and one on the western coast (Naples). For the currents, we used ADCP measurements from the University of South Florida's College of Marine Science's (USF/CMS) Coastal Ocean Monitoring and Prediction System (COMPS) for the WFS (Weisberg et al., 2009). More specifically, we used measurements from moorings C10, C12 and C13, respectively located at the 25, 50, and 50 m isobaths of the WFS (Liu et al., 2020). Finally, for the waves, we used measurements from four buoys of the NOAA's National Data Buoy Center (NDBC); two on Florida's eastern shelf and two on the WFS. The locations of all measurement stations are shown in Fig. 1A,C.

### *2.2. Wind and atmospheric pressure during Hurricane Irma*

Irma made landfall in Florida on 10 September 2017 as a category 3 hurricane, first at Cudjoe Key (Florida Keys) and later on Marco Island, south to Naples (see hurricane track in Fig. 1). It then weakened to a category 2 hurricane as it moved further inland (Pinelli et al., 2018). The storm damaged up to 75% of the buildings at its landfall point in the Florida Keys, making it one of the strongest and costliest hurricanes on record in the Atlantic basin (Xian et al., 2018; Zhang et al., 2019). The strongest reported wind speed was 50 m/s on Marco Island while the highest recorded storm surge was 2.3 m, although larger wind speed likely occurred in the Florida Keys (Pinelli et al., 2018). In order to reproduce the wind profile of Irma in our model, we used high-resolution H*Wind wind fields (Powell et al., 1998). As these data represent 1-min averaged wind speeds, we multiplied them by a factor 0.93 to obtain 10-min averaged wind speeds (Harper et al., 2010), which are more consistent with the time step of our model. Furthermore, H*Wind

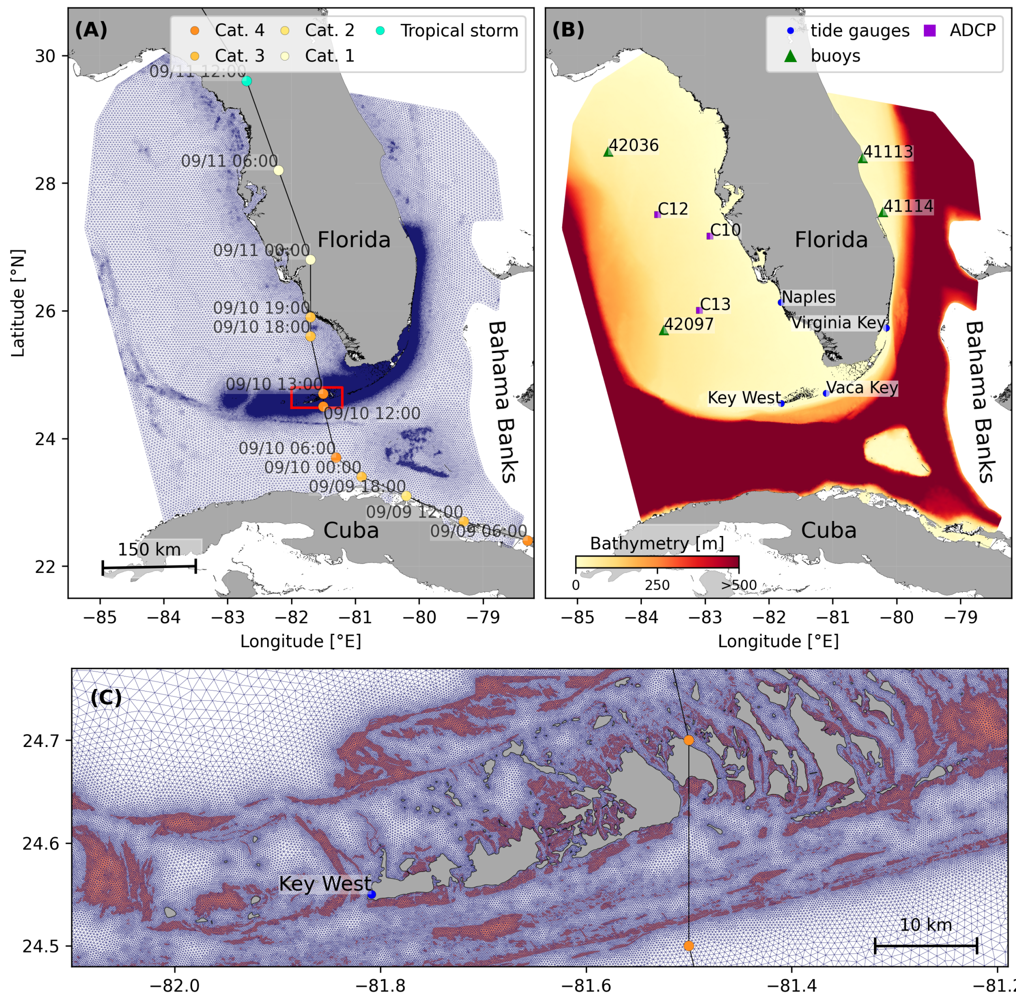


**Fig. 1:** (**A**) Mesh of the computational domain with the trajectory of Irma, category of the hurricane is given by the Saffir-Simpson color scale. (**B**) Bathymetry of the domain with the location of stations used for the validation of the model outputs. (**C**) Close up view of the Lower Keys area, where the mesh resolution reaches 100m near reefs (shown in dark orange) and islands (highlighted in dark grey)

wind profiles did not cover the whole model extent during the passage of the hurricane and were thus blended within coarser wind field extracted from ECMWF ERA-5 datasets (Fig. 2A). The pressure field during the passage of Hurricane Irma was also reconstructed using ERA-5 data. However, the coarse resolution of the dataset smoothes out the depression at the center of the hurricane, leading to an underestimation of the pressure gradient (Fig. 2B). To better capture the central depression of Irma, we therefore built a hybrid pressure field using the position and the minimal pressure of the core of the hurricane based on its track as recorded in the HURDAT 2 database (Landsea and Franklin, 2013). Based on this information, the hybrid pressure field was constructed by combining an idealized Holland pressure profile (Lin and Chavas, 2012) within the radius of maximum wind speed of Irma (Knaff et al., 2018) with ERA-5 pressure field. The transition from the Holland profile to ERA-5 data outside the radius of maximum wind speed data was performed using a smooth step function (Fig. 2).

### *2.3. Hydrodynamic model*

Ocean currents generated during hurricane Irma around South Florida were modelled using the 2D barotropic version of the unstructured-mesh coastal ocean model SLIM[1]. The model mesh covers an area similar to the model extent of Dobbelaere et al. (2020b), that includes the FRT but also the Florida Straits and part of the Gulf of Mexico (Figure 1). However, this area has been slightly extended northeastward and westward in order to include the NOAA-NDBC buoys. Furthermore, to withstand potential cell drying during the hurricane, we solved the conservative shallow water equations with

[1] `https://www.slim-ocean.be`

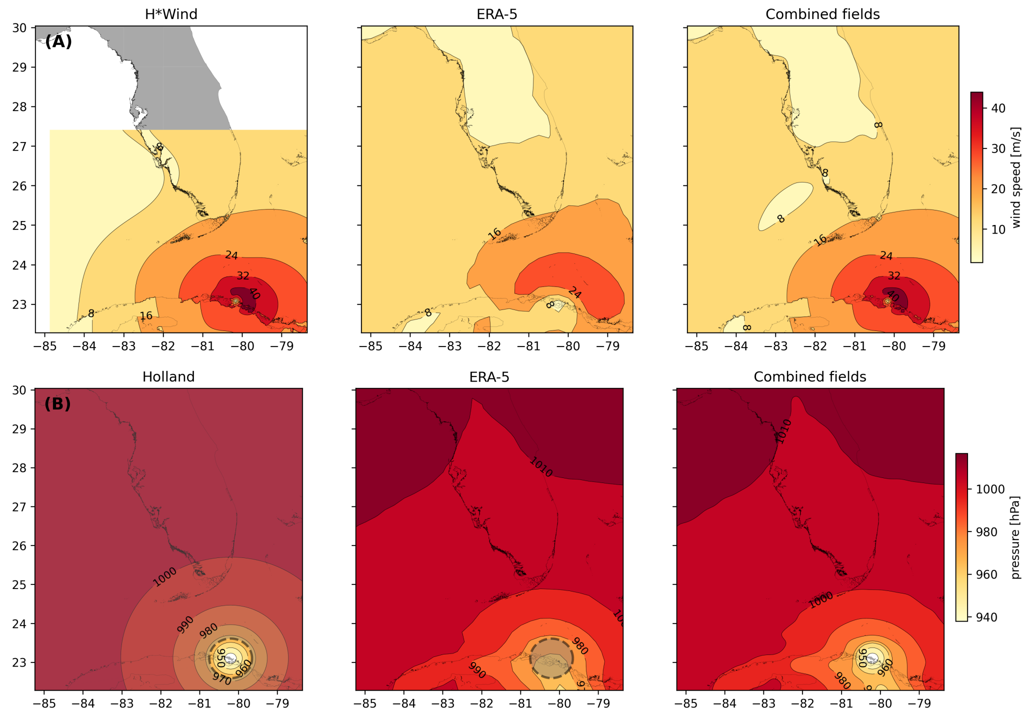


**Fig. 2:** Snapshot of the hybrid wind (**A**) and pressure (**B**) profiles constructed to capture the passage of Hurricane Irma at 1800 UTC on 9 September 2017. Wind profiles are obtained by combining high resolution H*Wind with coarser ERA-5 wind fields. The pressure field is built by combining the ERA-5 pressure field with an idealized Holland pressure profile based on the track of Irma in the HURDAT 2 database. Holland field was only used within the radius of maximum wind speed (dashed grey line) of the hurricane to capture its central depression.

wetting-drying:

$$
\begin{aligned}
\frac{\partial H}{\partial t} + \nabla \cdot (\mathbf{U}) &= 0 \ , \\
\frac{\partial \mathbf{U}}{\partial t} + \nabla \cdot \left( \frac{\mathbf{U}\mathbf{U}}{H} \right) &= -\, f\mathbf{e}_z \times \mathbf{U} + \alpha g H \nabla (H - h) - \frac{1}{\rho} \nabla p_{\mathrm{atm}} + \frac{1}{\rho} \boldsymbol{\tau}_s \\
&\quad + \nabla \cdot (\nu \nabla \mathbf{U}) - \frac{C_b}{H^2} |\mathbf{U}| \mathbf{U} + \gamma (\mathbf{U}_{\mathrm{ref}} - \mathbf{U}) \ ,
\end{aligned}
\tag{1}
$$

where $H$ is the water column height and $\mathbf{U}$ is the depth-averaged transport; $f$ is the Coriolis coefficient; $g$ is the gravitational acceleration; $h$ is the bathymetry; $\alpha$ is a coefficient stating whether the mesh element is wet ($\alpha = 1$) or dry ($\alpha = 0$) (Le et al., 2020); $\nu$ is the viscosity; $C_b$ is the bulk bottom drag coefficient; $p_{\mathrm{atm}}$ is the atmospheric pressure; $\boldsymbol{\tau}_s$ is the surface stress, usually due to wind; and $\gamma$ is a relaxation coefficient towards a reference transport $\mathbf{U}_{\mathrm{ref}}$. As in Frys et al. (2020) and Dobbelaere et al. (2020b), SLIM currents were gradually relaxed towards the operational Navy HYCOM product (GOMl0.04[2], Chassignet et al. (2007)) in regions where the water depth exceeds 50m.

At very high wind speeds, the white cap is blown off the crest of the waves. This phenomenon, also known as spumes, has been hypothesized to generate a layer of droplets that acts as a slip layer for the winds at the ocean-atmosphere interface (Holthuijsen et al., 2012). It causes a saturation of the wind drag coefficient for strong winds (Powell et al., 2003; Donelan et al., 2004; Curcic and Haus, 2020). We take this saturation effect into account by using the wind drag parameterization of Moon et al. (2007). In this parameterization, the drag coefficient $C_d$ depends on the wind speed at 10-m height $U_{10}$ according to:

$$
C_d = \kappa^2 \log \left( \frac{10}{z_0} \right)^{-2} \tag{2}
$$

[2] `https://www.hycom.org/data/goml0pt04`

where $\kappa$ is the von Karman constant and $z_0$ is the roughness length expressed as:

$$z_0 = \begin{cases} \dfrac{0.0185}{g} U_*^2 & \text{if } U_{10} \leq 12.5 \text{ m/s} \ , \\ [0.085(-0.56U_*^2 + 20.255U_* & \text{if } U_{10} > 12.5 \text{ m/s} \ , \\ \quad +2.458) - 0.58] \times 10^{-3} & \end{cases} \tag{3}$$

with $U_*$ the friction velocity. The relation between $U_{10}$ and $U_*$ is given by:

$$U_{10} = -0.56U_*^2 + 20.255U_* + 2.458 \ . \tag{4}$$

The mesh resolution depends on the distance to the coastlines and reefs following the approach of Dobbelaere et al. (2020b). The mesh is then further refined according to bathymetry value and gradient, as suggested in the SWAN user-guide[3]. Such an approach improves the model efficiency as the mesh resolution is only increased where required by the currents and waves dynamics. The mesh was generated with the seamsh[4] Python library, which is based on the the open-source mesh generator GMSH (Geuzaine and Remacle, 2009). It is composed of approximately $7.7 \times 10^5$ elements. The coarsest elements, far away from the FRT, has a characteristic length of about 5 km whereas the finest elements have a characteristic length of about 100 m along the coastlines and over the reefs (Fig 1).

### *2.4. Wave model*

Waves were modelled using the parallel unstructured-mesh version of the Simulating WAves Nearshore (SWAN) model (Booij et al., 1999), one of the most popular wave models for coastal areas and inland waters. It solves the action balance equation (Mei, 1989):

$$\frac{\partial N}{\partial t} + \nabla_{\mathbf{x}} \cdot [(\mathbf{c}_g + \mathbf{u})N] + \frac{\partial}{\partial \theta}[c_\theta N] + \frac{\partial}{\partial \sigma}[c_\sigma N] = \frac{S_{in} + S_{ds} + S_{nl}}{\sigma} \ , \tag{5}$$

[3]http://swanmodel.sourceforge.net/unswan/unswan.htm

[4]https://pypi.org/project/seamsh/

where $N = E/\sigma$ is the wave action density and $E$ is the wave energy spectrum; $\theta$ is the wave propagation direction; $\sigma$ is the intrinsic wave frequency; $\mathbf{c}_g$ is the wave group velocity, $\mathbf{u} = \mathbf{U}/H$ is SLIM depth-averaged current velocity; $c_\theta$ and $c_\sigma$ are the propagation velocities in spectral space due to refraction and shifting in frequency due to variations in depth and currents; and $S_{in}$, $S_{ds}$, and $S_{nl}$ respectively represent wave growth by wind, wave decay and nonlinear transfers of wave energy through interactions between triplets and quadruplets. The wave spectra were discretized with 48 direction bins and 50 frequency bins logarithmically distributed from 0.03 to 2 Hz. Exponential wind growth was parameterized using the formulation of Janssen (1991), while dissipations by whitecapping and bottom dissipations followed the formulations of Komen et al. (1984) and Madsen et al. (1989), respectively. Coefficients for exponential wind growth and whitecapping parameterizations were based on the results of Siadatmousavi et al. (2011), and significantly differ from SWAN's default settings. By default, SWAN implements the wind input formulation of Komen et al. (1984) and the steepness-dependent coefficient governing dissipation by whitecapping is a linear function of the wave number. In this study, this steepness-dependent coefficient is a quadratic function of the wave number, as it showed better predictions of the significant wave height in the study of Siadatmousavi et al. (2011). The choice of these formulations was motivated by the appearance of numerical instabilities in the region of the Gulf Stream when using SWAN's default parameter values. Finally, wave boundary conditions were derived from WAVEWATCH III (Tolman et al., 2009) spectral outputs at NDBC buoy locations. We selected these datasets as the large number of NDBC buoys around our region of interest allowed for a fine representation of the wave spectra on the boundary of the domain.

Surface waves induce a net drift in the direction of the wave propagation, known as the Stokes drift (Van Den Bremer and Breivik, 2018; Stokes, 1880). This net drift has a significant impact on sediment transport in nearshore regions (Hoefel and Elgar, 2003), on the formation of Langmuir cells (Langmuir, 1938; Craik and Leibovich, 1976) as well as on the transport of heat, salt or pollutants such as oil or micro-plastic in the upper ocean layer (McWilliams and Sullivan, 2000; Röhrs et al., 2012; Drivdal et al., 2014). To correctly model the Stokes drift profile in mixed wind-driven sea and swell conditions, the full two-dimensional wave spectrum must be represented by a spectral wave model within a wave-current coupling (Van Den Bremer and Breivik, 2018). We therefore used SWAN modelled spectra to compute the Stokes drift as follows:

$$\mathbf{u}_s = \int_0^{2\pi} \int_0^{+\infty} \frac{\sigma^3}{h \tanh(2kh)} E(\sigma, \theta)(\cos\theta, \sin\theta) d\sigma d\theta \ , \tag{6}$$

where $k$ is the norm of the wave vector; $h$ is the water depth; and $E(\sigma, \theta)$ is the wave energy density.

### *2.5. Coupled model*

SLIM and SWAN are coupled so that they run on the same computational core and the same unstructured mesh. SLIM is run first and passes the wind velocity ($\mathbf{U}_{10}$), water level ($\eta = H - h$) and depth-averaged current ($\mathbf{u} = \mathbf{U}/H$) fields to SWAN, as well as a roughness length ($z_0$) for the bottom dissipation formulation of Madsen et al. (1989). This roughness length is computed from SLIM's bulk drag coefficient $C_b$ following the approach of Dietrich et al. (2011) so that both models have consistent bottom dissipation parameterizations. SWAN then uses these quantities to compute the wave radiation stress gradient, that is then passed to SLIM as the force exerted by waves on currents $\boldsymbol{\tau}_{\text{wave}}$ (Fig. 3). SLIM then uses this quantity to update the value of the surface stress $\boldsymbol{\tau}_s$ in Eq. (1), that now becomes the sum of wind and wave-induced stresses $\boldsymbol{\tau}_s = \boldsymbol{\tau}_{\text{wind}} + \boldsymbol{\tau}_{\text{wave}}$. Here, the momentum flux from the atmosphere to the ocean is taken as the commonly-used full wind tress $\boldsymbol{\tau}_{\text{wind}}$. Doing so, we neglect the momentum advected away from the storm by the waves, leading to a 10-15% overestimation of the momentum flux in hurricane winds (Curcic, 2015). Moreover, we followed the approach of Dietrich et al. (2012) by characterizing the wave-induced stresses using the radiation-stress representation instead of the vortex-force representation (McWilliams et al., 2004). Although the later provides a clearer and more meaningful decomposition of the wave effect, we implemented the first representation for the sake of simplicity as it allows us to provide the whole wave contribution as an additional surface stress to SLIM (Lane et al., 2007).

SLIM's governing equations are integrated using an implicit time integration scheme while SWAN is unconditionally stable (Dietrich et al., 2012), allowing both models to be run with relatively large time steps. In this study, the stationary version of SWAN was used, *i.e.* the time derivative of Eq. 5 was set to zero. This resulted in reduced scaling and convergence rates than with the nonstationary version of SWAN but increased the stability of the model. The wave spectra at each node of the mesh was saved at the end of each iteration to serve as initial conditions for the next one. Both models were run sequentially using a time step of 600 s, so that each computational core was alternatively running either SLIM or SWAN. As in the coupling between SWAN and ADCIRC (Dietrich et al., 2012), both models use the same local sub-mesh, allowing for a one-to-one correspondence between the geographic locations of the mesh vertices. No interpolation is therefore needed when passing the discretised variables from one model to the other, which allows an efficient inter-model communication. However, as SLIM is based on a discontinuous Galerkin finite element method, an additional conversion step to a continuous framework was required to transfer SLIM nodal quantities to SWAN.

### *2.6. Quantifying the effect of wave-current interactions on transport*

To quantify the impact of wave-current interactions on transport processes, we compared the trajectories of passive particles advected by the uncoupled SLIM and coupled SLIM+SWAN currents during the passage of Irma in the

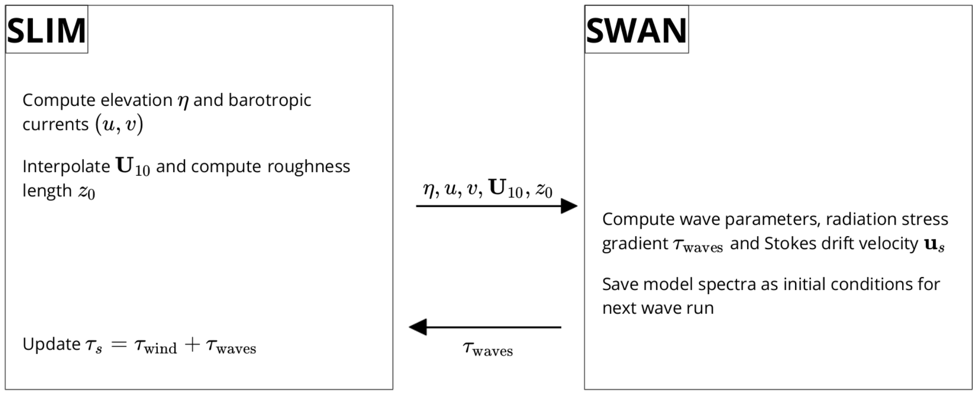


**Fig. 3:** Schematic illustration of the coupled SLIM+SWAN model.

Lower Keys. Furthermore, the depth-averaged Stokes drift was computed using the wave spectra of the coupled model SLIM+SWAN run as well as those of an uncoupled SWAN run. Particles were released on the inner and outer shelves at the points highlighted By red and blue dots in Fig. 4 on Sept. 7 at 0000 UTC and then tracked until Sept. 15. These initial particle positions were found using backtracking methods (Dobbelaere et al., 2020a) to ensure that the release particles would intersect the path of Irma during its passage through the Florida Keys. We first defined two 25 km$^2$ circular regions on the trajectory of the hurricane (see red and blue circles in Fig. 4). Particles within these two regions were then tracked backward in time using uncoupled SLIM currents from the exact time of the passage of the hurricane until Sept. 7 at 0000 UTC. Their positions at the end of the backward simulation (see red and blue particle clouds in Fig. 4) corresponds to the initial condition of the forward transport simulations described below. We then compared the trajectories of particles originating from these regions and advected forward in time by different sets of currents: (i) uncoupled SLIM currents alone; (ii) coupled SLIM+SWAN currents; (iii) SLIM currents with the addition of the depth-averaged Stokes drift computed with the coupled wave-current model (Stokes-C); (iv) SLIM+SWAN currents with Stokes-C;

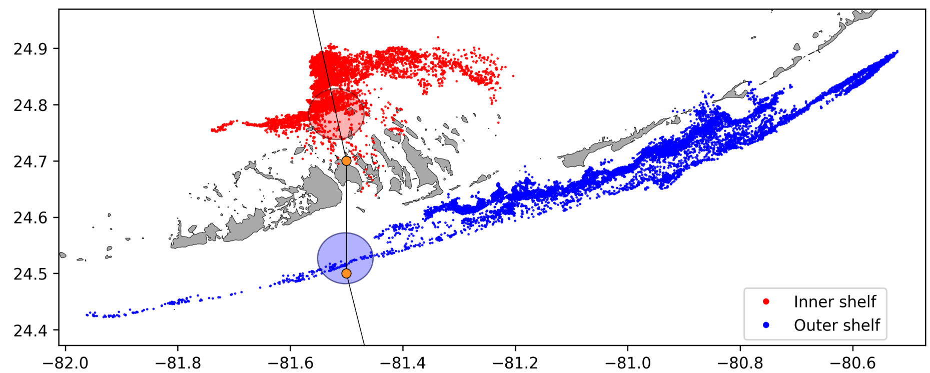


**Fig. 4:** Release regions of the passive particles on the inner and outer shelves (red and blue clouds) obtained by backtracking particles released in the red and blue circular areas during the passage of Irma.

and (v) SLIM currents with the depth-averaged Stokes drift computed with the uncoupled wave model (Stokes-U). Particles trajectories are compared by computing the distances between the centers of mass of the particle clouds through time.

## 3. Results

We first validated the reconstructed atmospheric fields of hurricane Irma as well as the outputs of our coupled wave-current model against field measurements. A summary of the error statistics is given in Table 1. We then used the validated model outputs to simulate the transport of passive drifters in the Lower Keys during the passage of Hurricane Irma. These drifters were advected by the sets of currents described in section 2.6 and their trajectories were compared to evaluate the impact of the wave-current interactions and the Stokes drift on the transport processes during the passage of Irma.

### *3.1. Model validation*

H*Wind winds and hybrid pressure field agree well with station measurements at Vaca Key station (Fig. 5). The hybrid pressure field shows a

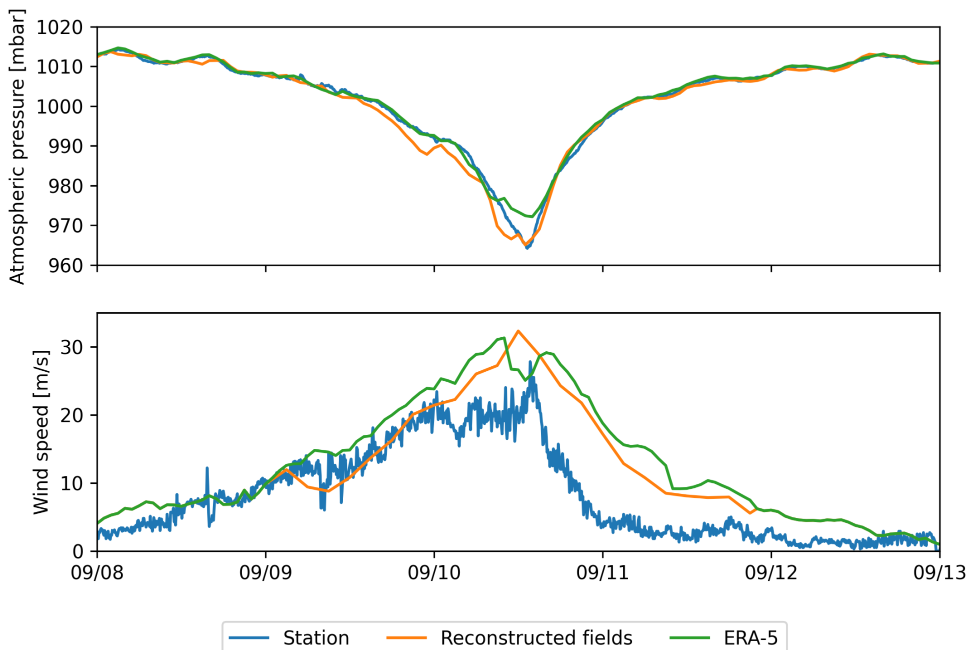


**Fig. 5:** Comparison of reconstructed wind atmospheric pressure with field measurements and coarser ECMWF ERA-5 profiles at Vaca Key station. The generated hybrid atmospheric forcings better reproduce the observed storm depression while H*wind winds better reproduce the measured peak in wind speed.

better agreement with observations than ERA-5 pressure as it successfully reproduces the storm depression. ERA-5 fields, on the other hand, fail to reproduce the low pressure at the core of the hurricane due to their coarser grid, leading to an overestimation of 8 mbar of the storm depression. Both H*Wind and ERA-5 agree well with observed wind speeds although both data sets tend to slightly overestimate the width and intensity of the wind peak. However, H*wind profiles better reproduce the timing of the observed peak, as ERA-5 winds tend to anticipate it. H*wind also exhibits a slightly narrower peak in wind speed, which better agrees with observations.

Hydrodynamic outputs of the coupled wave-current model agree well with tide gauge (Fig. 6) and ADCP measurements (Fig. 7). Despite a slight overestimation of the amplitude of sea surface elevation (Table 1) in fair weather conditions, the timing and amplitude of the storm surges are well reproduced by the coupled model. The largest model error during the surge is an overestimation of 18 cm of the elevation peak at Virginia Key. The fit is especially good at Naples, where both the large positive and negative surges are captured by the coupled model with an error of less than 5 cm. Modelled 2D currents were validated against depth-averaged ADCP measurements at mooring stations C10, C12 and C13 (Fig. 7). As in Liu et al. (2020), we performed the vector correlation analysis of Kundu (1976) to compare modelled and observed current velocity vectors. Correlation coefficients ($\rho$) between simulated and observed depth-averaged currents are 0.84, 0.74 and 0.73 at stations C10, C12 and C13, respectively. Average veering angles were computed as well and are below 12°, as in (Liu et al., 2020). Furthermore, the positive bias in Table 1 indicates that our model tends to underestimate the southward component of the currents at the different stations. As expected from a depth-averaged model, the best fit with observations is obtained at the shallowest mooring C10, located on the 25 m isobath, with an average veering angle of 6° and smaller error statistics (Table 1).

The simulated significant wave height agrees well with observations on the WFS, where errors on the peak value do not exceed 5% (Fig. 8). On Florida's eastern shelf, errors are slightly larger and reach 20%. Although the model outputs agree well with observations, a lag in significant wave height is observed for all 4 buoys. Moreover, the peak in significant wave height tends to be underestimated at buoys 41113 and 41114, located on the East Florida Shelf. Other wave parameters were better reproduced by the model on the WFS as well (see buoy 42036 in Fig. 8 and Table 1).

### *3.2. Impact of waves on currents and transport*

We evaluated the impact of wave-current interactions on modelled currents during the passage of Irma in the Lower Keys, between Sept. 7 and 13, 2017. First, we computed the maximum difference between currents modelled by SLIM and SLIM+SWAN during this period (Fig. 9A). The largest differences

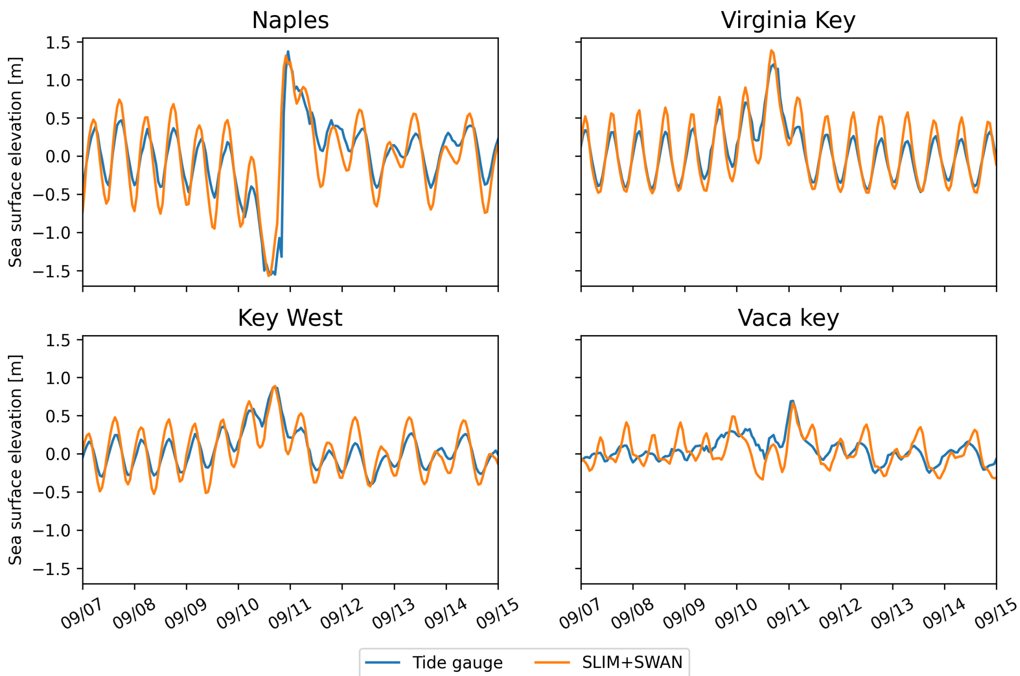


**Fig. 6:** Comparison of modelled sea surface elevation at the 4 tide gauges shown in Fig. 1B. The timing and amplitudes of the storm surges are well reproduced by the model

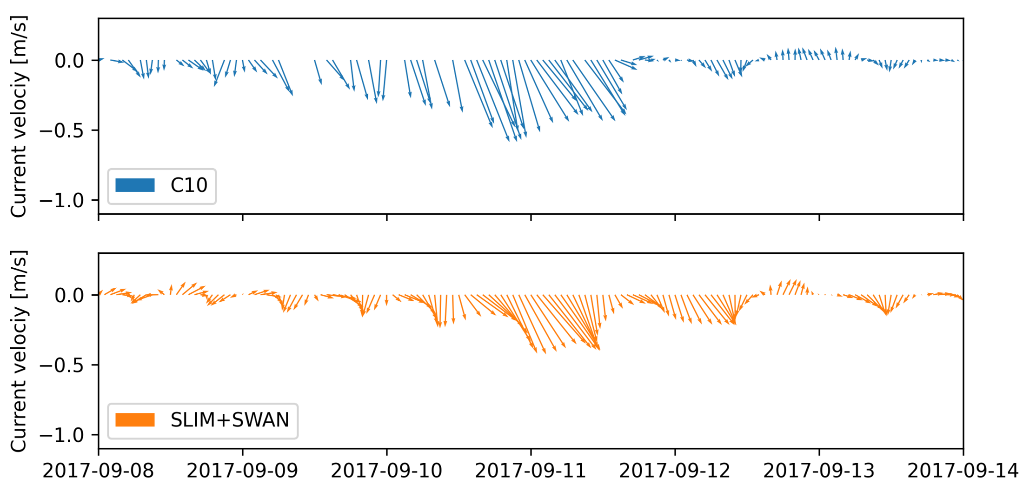


**Fig. 7:** Comparison of modelled current velocity with observed velocity at mooring C10 (see Fig. 1B for its location). Modelled current velocities agree well with observations, with a correlation coefficient of 0.83 and an average veering angle of 6°.

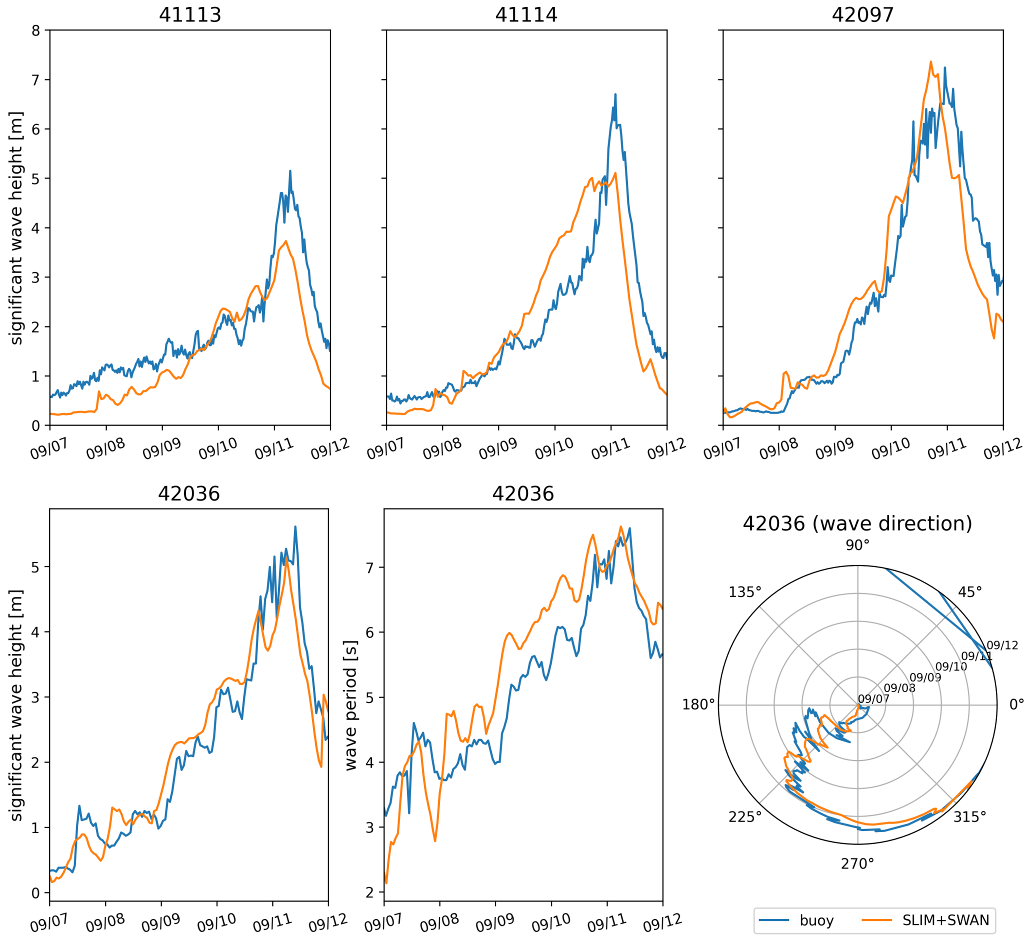


**Fig. 8:** Comparison of modelled wave parameters with observation at the 4 buoys location (locations shown in Fig. 1B). Modelled significant wave height agrees well with field measurement.

| **Station** | **Variable** | **Bias** | **MAE** | **RMSE** |
|---|---|---|---|---|
| Vaca Key | sse (m) | n/a | 0.12 | 0.16 |
| | $U_{10}$ (m/s) | 1.51 | 1.85 | 2.61 |
| | $p_{\mathrm{atm}}$ (hPa) | -0.21 | 0.59 | 1.03 |
| Key West | sse (m) | n/a | 0.11 | 0.13 |
| Virginia Key | sse (m) | n/a | 0.10 | 0.13 |
| Naples | sse (m) | n/a | 0.18 | 0.23 |
| C10 | $u$ (m/s) | -0.006 | 0.04 | 0.05 |
| | $v$ (m/s) | 0.02 | 0.06 | 0.08 |
| C12 | $u$ (m/s) | -0.01 | 0.06 | 0.07 |
| | $v$ (m/s) | 0.06 | 0.09 | 0.11 |
| C13 | $u$ (m/s) | 0.004 | 0.06 | 0.08 |
| | $v$ (m/s) | 0.04 | 0.06 | 0.08 |
| 41113 | $H_s$ (m) | -0.35 | 0.40 | 0.51 |
| | $T_m$ (s) | -2.18 | 2.47 | 3.13 |
| 41114 | $H_s$ (m) | -0.21 | 0.53 | 0.68 |
| | $T_m$ (s) | -1.69 | 2.53 | 3.15 |
| 42036 | $H_s$ (m) | -0.03 | 0.26 | 0.36 |
| | $T_m$ (s) | 0.04 | 0.65 | 0.77 |
| 42097 | $H_s$ (m) | -0.15 | 0.40 | 0.57 |
| | $T_m$ (s) | 0.02 | 0.62 | 0.74 |

Table 1: Error statistics comparing SLIM+SWAN simulated quantities with the measured sea surface elevation (sse), eastward and northward depth-average current velocities ($u$,$v$), significant wave height ($H_s$), and zero-crossing mean wave period ($T_m$). Model bias, mean absolute error (MAE), and root mean squared error (RMSE) are listed by variable (unit) and value.

in current speed were observed over the reefs, on the shelf break and around islands. They can locally reach 1 m/s, with the coupled SLIM+SWAN model yielding the largest amplitudes. The regions where the differences are the largest experience the strongest radiation-stress gradient $\boldsymbol{\tau}_{\text{wave}}$ (Fig. 9B) induced by wave energy dissipation on the shelf-break and rough seabed induce variations of the wave radiation stress (Longuet-Higgins and Stewart, 1964). This highlights the important protective role of the barrier formed by the offshore reefs, that require a fine spatial resolution to be accurately captured. Wave-induced differences in current speed were amplified by the action of the wind stress $\boldsymbol{\tau}_{\text{wind}}$ (Fig. 9C). Wind speeds were larger in the front right quadrant of the hurricane (Zedler et al., 2009), yielding larger differences on the right-hand side of the storm trajectory. This is especially clear in the area between the Florida Keys and the Everglades, where relatively small values of $\boldsymbol{\tau}_{\text{wave}}$ nonetheless produce current speed differences of up to 0.5 m/s because of the wind stress.

Waves play a significant role on the transport processes during and after the passage of hurricane Irma (Fig. 10A). Comparing SLIM and SLIM+SWAN shows that wave-current interactions alone yield differences of up to 5 km between the modelled trajectories on the passage of the hurricane. These differences exceed 10 km on the outer shelf when Stokes drift is taken into account. The impact of the waves on the transport processes differs significantly between the inner and outer shelves, with wave-induced differences in trajectories 4 to 5 times larger on the outer shelf. Furthermore, the distances between the centers of mass of the clouds of particles tend to stabilize on the inner shelf after the passage of Irma, while they keep increasing on the other shelf up to two days after the passage of the hurricane when taking Stokes drift into account. These distances then stabilize for about a day before they start decreasing (see right panel of Fig. 10A). However, when considering wave-current interactions alone (SLIM vs. SLIM+SWAN), the distance between the clouds of particles starts to decrease just after the

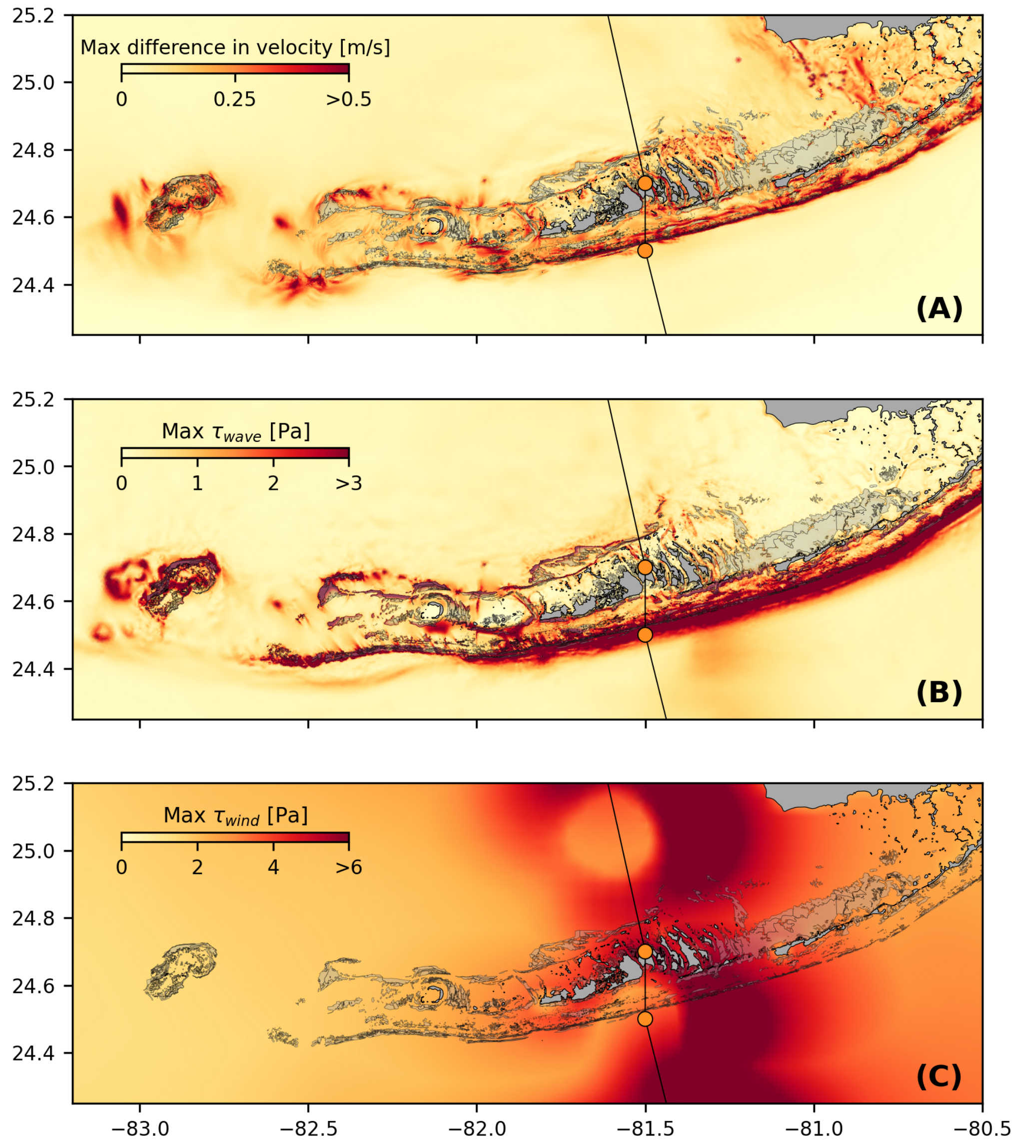


**Fig. 9:** (**A**). Maximum difference between SLIM and SLIM+SWAN currents during the passage of Irma in the Lower Florida Keys; (**B**) Maximum wave radiation stress gradient $\boldsymbol{\tau}_{\text{wave}}$ and (**C**) maximum wind stress $\boldsymbol{\tau}_{\text{wind}}$ (**C**) generated by the hurricane. Radiation stress gradient yields difference larger than 0.5 m/s in current velocities, especially over offshore reefs.

passage of Irma.

The Stokes drift appears to have a larger effect than the radiation stress gradient and the wave-current interactions (Fig 10A). Nonetheless, comparing the different curves for the outer shelf suggests that the radiation-stress gradient induces effects similar to the impact of the Stokes drift in this region during the passage of Irma. However, comparing SLIM and SLIM+SWAN both on the inner and other shelf, we see that this impact is negligible during the rest of the simulation. Moreover, comparison of Stokes-U and Stokes-C (Fig. 10B) indicates that the difference between the trajectories of particles advected by the two Stokes drift do not exceed 2 km, with larger discrepancies on the outer shelf. The sudden increase of 'SLIM+Stokes-C vs SLIM+Stokes-U' curves on the passage of Irma (and two days after on the outer shelf) and their stabilization afterwards suggest that taking wave-currents interactions into account when modeling waves mostly has an impact during (and directly after) the passage of the hurricane.

## 4. Discussion

Validation against field measurements show that the coupled SLIM+SWAN model correctly reproduce hydrodynamics and wave dynamics during hurricane Irma. Such good agreement is obtained using accurate forcings and adequate wave parameterizations. Furthermore, comparing coupled and uncoupled model runs suggests that neglecting wave radiation stress gradient induces differences of up to 1 m/s in modeled current velocities. Radiation stress gradient during the hurricane was especially large over the shelf break, where waves are strongly dissipated by the protective coral barrier and can lead to variations of more than 10 km in modelled trajectories. These differences in modelled trajectories were significantly larger and required more time to stabilize on the outer shelf. The impact of the Stokes drift dominates the effects of wave-current interactions through the radiation stress gradient, except at the moment of the passage of the hurricane, when both contributions

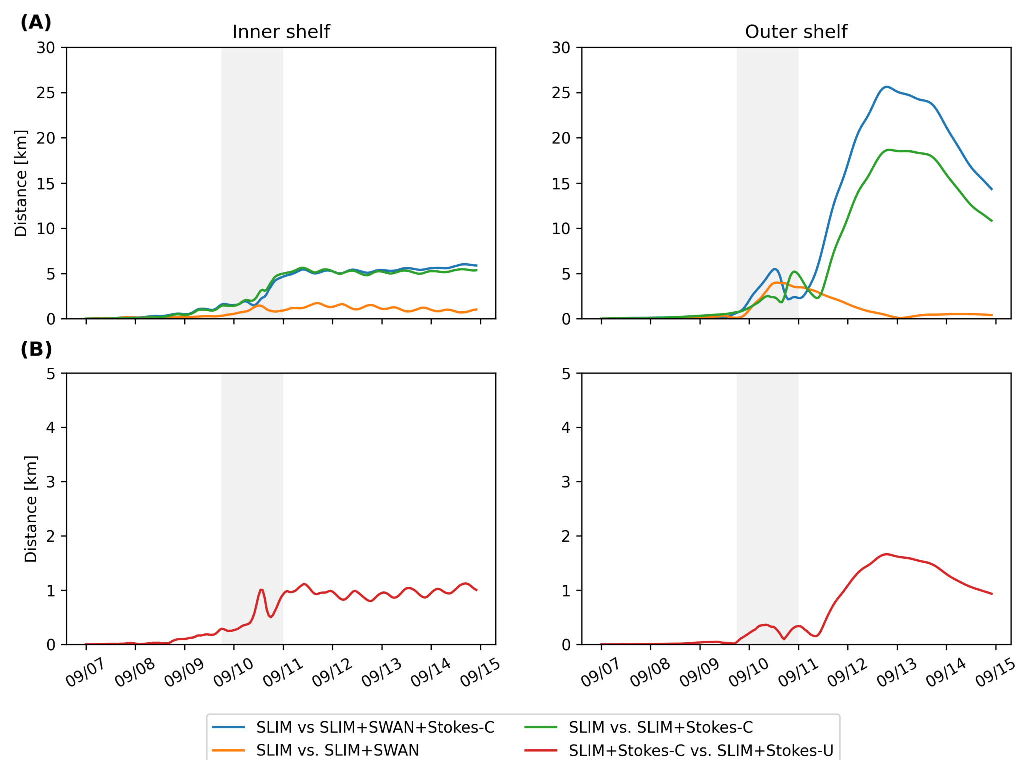


**Fig. 10:** Difference between the centers of mass of the particle clouds released from the regions highlighted in Fig. 4 and advected by different combinations of coupled and uncoupled velocity fields.

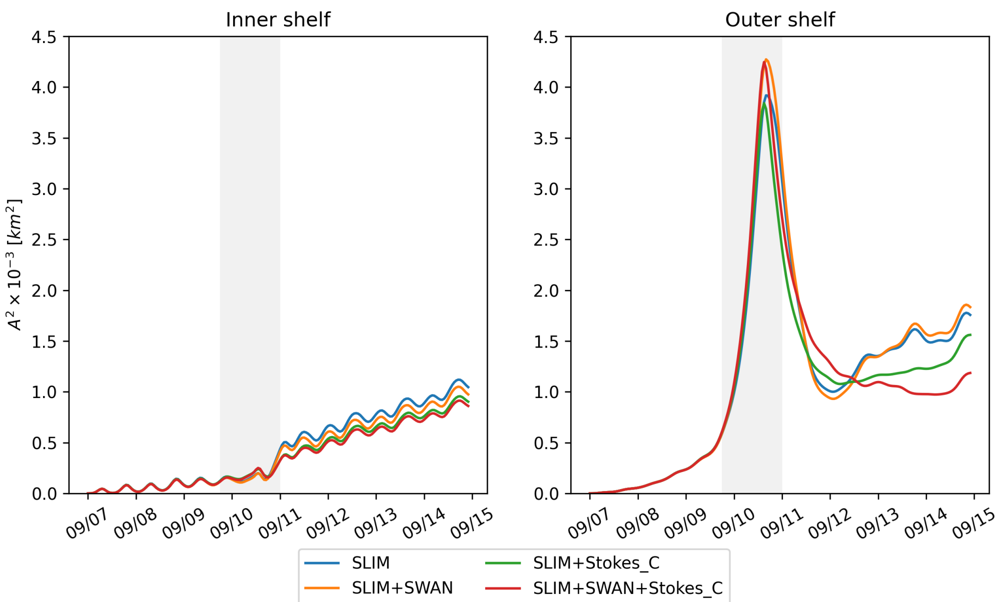


**Fig. 11:** Dispersion of particles with different velocity fields → not sure to know what to say about that...

are similar. Finally, neglecting wave-current interactions when computing Stokes drift lead to variations of up to 2 km in modelled trajectories on the passage of the hurricane.

Despite slightly overestimating the amplitude of the sea surface elevation in fair weather conditions, the coupled model reproduces correctly the timing and amplitude of the observed storm surge (Fig. 6). All elevation peaks are captured with a 4% accuracy at every stations except Virginia key, where the surge was overestimated by about 15%. Such accuracy is key to predict the damages caused by the hurricane, as most destroyed and severely damaged buildings in the Florida keys during Hurricane Irma were caused by storm surge and waves (Xian et al., 2018). Furthermore, the high resolution of model in the regions captures flow accelerations between islands and reefs, allowing for a precise representation of the surge risk in the Florida Keys. In addition to accurately capture positive surges, the model also reproduced the observed negative surge in Naples with an error of about 1%. This result is of interest from a biological point of view as negative surges, although less studied, affect water exchanges between the estuaries and the coastal ocean and disturb the benthic ecosystems (Liu et al., 2020). Such rapid decrease in water level followed by a positive surge cause massive freshwater inflows, generating a significant decrease in water salinity (Wachnicka et al., 2019).

Strong currents such as the Gulf Stream affect waves trough refraction over gradients in current velocity, shoaling and breaking of opposing waves or lengthening of following waves (Hegermiller et al., 2019). Under hurricane conditions, these interactions can cause numerical instabilities in the wave model if appropriate parameterizations and model resolution are not applied. Hegermiller et al. (2019), for instance, used a 5-km model grid and 48 directional bins to capture spatial gradients in wave height induced by wave-currents interactions in the Gulf Stream during Hurricane Matthew (2016). These guidelines were followed when defining the coarsest resolution of the model mesh as well as the spectral discretization of SWAN. Boundary conditions and directional spreading of the incident waves also play a significant role when modeling wave-current interactions at meso- and submesoscales (Villas Bôas et al., 2020), which motivated our choice of imposing full spectra on the boundary of the wave model instead of bulk parameters. Finally, SWAN default parameterizations for wind energy input and whitecapping caused numerical instabilities by overestimating wave growth and steepness on the boundary of the Gulf Stream on the passage of Irma. This overestimation was solved by using the parameterization of Siadatmousavi et al. (2011). The parameters used in this study were calibrated on the Northern Gulf of Mexico, which might explains that our model better reproduces wave parameters at buoys 42036 and 4207, located on the WFS. However, these calibrated parameters might underestimate wind-induced wave growth might underestimate Florida's eastern shelf. Consequently, incident wave do not receive enough energy to grow after breaking on the bank boundary, leading to the underestimation of the significant wave height at buoys 41113 and 41114. A more extensive calibration study might therefore be necessary to achieve good agreement with field measurements on both sides of Florida. Nonetheless, as this study focuses on the wave produced by Irma, which made landfall on the western coasts of Florida, the use of parameterizations calibrated for the Gulf of Mexico seems reasonable.

Radiation stress gradient significantly impacts currents during the passage of the hurricane. It can induce differences of up to 1 m/s of the current velocity on the shelf break. In this region waves are strongly dissipated due to action of depth-induced breaking and bottom dissipation on the coral reefs. This highlights the efficiency of the reefs as a protective barrier against strong waves. Moreover, it advocates for the use of a high spatial resolution in this region in order to accurately capture the impact of these reefs. Due to the dissipation of incoming waves on the coral barrier, wave impact during Irma is different on the inner and outer shelves. It is less important on the inner shelf because of the sheltering of the inner shelf due to reefs and islands as well as wave breaking on the shelf break. The inner shelf hence experiences weaker waves and currents, inducing weaker and more localized transport. Furthermore, the impact of winds on waves is reduced in shallower areas under the action of depth-induced breaking. This might explain why differences between particle trajectories stabilize on the inner shelf just after the passage of Hurricane Irma. However, the Florida Keys still experienced strong winds after the passage of the core of the hurricane, which generated high waves in the deeper areas. This might explain why the differences on between the modelled trajectories kept increasing on the outer shelf under the action of strong Stokes drift up to two days after the passage of the hurricane.

The distance between the centers of mass of clouds of particles coupled and uncoupled Stokes drift did not exceed 2 km (Fig. 10). This suggest that taking wave-currents interactions into account when computing Stokes drift, even under hurricane conditions yields a limited impact. Furthermore, combining the coupled Stokes drift with the coupled and uncoupled SLIM currents produced similar trajectories on the inner shelf, which seems to indicate that wave impact of currents is limited in this region. This would suggest that it is not necessary to take wave-current interactions into account when modeling the trajectories of tracers in shallow, sheltered areas such as the inner WFS during a hurricane. Uncoupled currents with uncoupled Stokes drift should give a reasonably accurate approximation of the transport processes. However, this does not hold for deeper regions, as highlighted by the comparison of trajectories obtained with coupled and uncoupled SLIM currents combined with coupled Stokes drift on the outer shelf.

## 5. Conclusion

We developed a coupled wave-current model to study the impact of waves on transport processes during Hurricane Irma. In order to accurately represent the wind and pressure profiles of te hurricane, we built hybrid fields by combining coarser ERA-5 data with high-resolution H*Wind data for the wind speed and idealized Holland profiles for the pressure. Comparing these hybrid profiles with field observations showed that they were better at reproducing the observed central depression of the hurricane as well as the peak in wind speed than ERA-5 data. Using these hybrid fields as forcings, our coupled model accurately reproduced the storm surge at NDBC buoy locations and produced currents and wave parameters in good agreement with field observations, especially on the WFS. The modelled currents and Stokes drift were then used to evaluate the impact of waves on the trajectory of passive drifters on the passage of the hurricane through the Florida Keys.

Despite its good agreement with observations, our model lacks in the representation of the wind-wave interactions. In particular, it does not consider the momentum loss due to the action of surface waves when representing momentum flux from the atmosphere to the ocean, leading to overestimations under hurricane conditions. Our model could therefore be further improved by using wave-dissipative stress instead of the full wind stress as the momentum flux from the atmosphere to the ocean. Moreover, a more thorough calibration of the wave model parameters should improve our model results on the eastern shelf of Florida.

Wave coupling needs to be taken into account during heavy-wind events but not necessarily in milder conditions. While the wave-current interaction plays an important role and can lead to differences of up to [insert value], the Stokes drift is about [insert value] more intense and should thus be considered in priority

## Acknowledgments

Computational resources were provided by the Consortium des Équipements de Calcul Intensif (CÉCI), funded by the F.R.S.-FNRS under Grant No. 2.5020.11. Thomas Dobbelaere is a PhD student supported by the Fund for Research training in Industry and Agriculture (FRIA/FNRS).

## References

Bever, A.J., MacWilliams, M.L., 2013. Simulating sediment transport processes in San Pablo Bay using coupled hydrodynamic, wave, and sediment transport models. Marine Geology 345, 235–253.

Bhatia, K.T., Vecchi, G.A., Knutson, T.R., Murakami, H., Kossin, J., Dixon, K.W., Whitlock, C.E., 2019. Recent increases in tropical cyclone intensification rates. Nature Communications 10, 1–9.

Booij, N., Ris, R.C., Holthuijsen, L.H., 1999. A third-generation wave model for coastal regions: 1. Model description and validation. Journal of Geophysical Research: Oceans 104, 7649–7666.

Breivik, Ø., Allen, A.A., Maisondieu, C., Olagnon, M., 2013. Advances in search and rescue at sea. Ocean Dynamics 63, 83–88.

Chassignet, E.P., Hurlburt, H.E., Smedstad, O.M., Halliwell, G.R., Hogan, P.J., Wallcraft, A.J., Baraille, R., Bleck, R., 2007. The HYCOM (hybrid coordinate ocean model) data assimilative system. Journal of Marine Systems 65, 60–83.

Chen, C., Huang, H., Beardsley, R.C., Liu, H., Xu, Q., Cowles, G., 2007. A finite volume numerical approach for coastal ocean circulation studies: Comparisons with finite difference models. Journal of Geophysical Research: Oceans 112.

Craik, A.D., Leibovich, S., 1976. A rational model for Langmuir circulations. Journal of Fluid Mechanics 73, 401–426.

Curcic, M., 2015. Explicit air-sea momentum exchange in coupled atmosphere-wave-ocean modeling of tropical cyclones. Ph.D. thesis.

Curcic, M., Chen, S.S., Özgökmen, T.M., 2016. Hurricane-induced ocean waves and stokes drift and their impacts on surface transport and dispersion in the Gulf of Mexico. Geophysical Research Letters 43, 2773–2781.

Curcic, M., Haus, B.K., 2020. Revised estimates of ocean surface drag in strong winds. Geophysical Research Letters 47, e2020GL087647.

Dietrich, J., Bunya, S., Westerink, J., Ebersole, B., Smith, J., Atkinson, J., Jensen, R., Resio, D., Luettich, R., Dawson, C., et al., 2010. A high-resolution coupled riverine flow, tide, wind, wind wave, and storm surge model for southern Louisiana and Mississippi. Part II: Synoptic description and analysis of Hurricanes Katrina and Rita. Monthly Weather Review 138, 378–404.

Dietrich, J., Westerink, J., Kennedy, A., Smith, J., Jensen, R., Zijlema, M., Holthuijsen, L., Dawson, C., Luettich, R., Powell, M., et al., 2011. Hurricane Gustav (2008) waves and storm surge: Hindcast, synoptic analysis, and validation in southern louisiana. Monthly Weather Review 139, 2488–2522.

Dietrich, J.C., Tanaka, S., Westerink, J.J., Dawson, C., Luettich, R., Zijlema, M., Holthuijsen, L.H., Smith, J., Westerink, L., Westerink, H., 2012. Performance of the unstructured-mesh, SWAN+ ADCIRC model in computing hurricane waves and surge. Journal of Scientific Computing 52, 468–497.

Dobbelaere, T., Muller, E., Gramer, L., Holstein, D., Hanert, E., 2020a. Report on the potential origin of the SCTLD in the Florida Reef Tract. Available online at: `https://floridadep.gov/rcp/coral/documents/report-potential-origin-sctld-florida-reef-tract`.

Dobbelaere, T., Muller, E.M., Gramer, L.J., Holstein, D.M., Hanert, E., 2020b. Coupled epidemio-hydrodynamic modeling to understand the spread of a deadly coral disease in Florida. Frontiers in Marine Science 7, 1016.

Donelan, M., Haus, B., Reul, N., Plant, W., Stiassnie, M., Graber, H., Brown, O., Saltzman, E., 2004. On the limiting aerodynamic roughness of the ocean in very strong winds. Geophysical Research Letters 31.

Drivdal, M., Broström, G., Christensen, K., 2014. Wave-induced mixing and transport of buoyant particles: Application to the Statfjord A oil spill. Ocean Science 10, 977–991.

Figueiredo, J., Baird, A.H., Connolly, S.R., 2013. Synthesizing larval competence dynamics and reef-scale retention reveals a high potential for self-recruitment in corals. Ecology 94, 650–659.

Frys, C., Saint-Amand, A., Le Hénaff, M., Figueiredo, J., Kuba, A., Walker, B., Lambrechts, J., Vallaeys, V., Vincent, D., Hanert, E., 2020. Fine-scale coral connectivity pathways in the Florida Reef Tract: Implications for conservation and restoration. Frontiers in Marine Science 7, 312.

Geuzaine, C., Remacle, J.F., 2009. Gmsh: A 3-d finite element mesh generator with built-in pre-and post-processing facilities. International journal for numerical methods in engineering 79, 1309–1331.

Harper, B., Kepert, J., Ginger, J., 2010. Guidelines for converting between various wind averaging periods in tropical cyclone conditions.

Hegermiller, C.A., Warner, J.C., Olabarrieta, M., Sherwood, C.R., 2019. Wave–current interaction between Hurricane Matthew wave fields and the Gulf Stream. Journal of Physical Oceanography 49, 2883–2900.

Hoefel, F., Elgar, S., 2003. Wave-induced sediment transport and sandbar migration. Science 299, 1885–1887.

Holthuijsen, L.H., Powell, M.D., Pietrzak, J.D., 2012. Wind and waves in extreme hurricanes. Journal of Geophysical Research: Oceans 117.

Janssen, P.A., 1991. Quasi-linear theory of wind-wave generation applied to wave forecasting. Journal of Physical Oceanography 21, 1631–1642.

Johns, W.E., Schott, F., 1987. Meandering and transport variations of the Florida Current. Journal of Physical Oceanography 17, 1128–1147.

Knaff, J.A., Sampson, C.R., Musgrave, K.D., 2018. Statistical tropical cyclone wind radii prediction using climatology and persistence: Updates for the western North Pacific. Weather and Forecasting 33, 1093–1098.

Knutson, T., Camargo, S.J., Chan, J.C., Emanuel, K., Ho, C.H., Kossin, J., Mohapatra, M., Satoh, M., Sugi, M., Walsh, K., et al., 2020. Tropical cyclones and climate change assessment: Part ii: Projected response to anthropogenic warming. Bulletin of the American Meteorological Society 101, E303–E322.

Komen, G., Hasselmann, S., Hasselmann, K., 1984. On the existence of a fully developed wind-sea spectrum. Journal of Physical Oceanography 14, 1271–1285.

Kossin, J.P., Knapp, K.R., Olander, T.L., Velden, C.S., 2020. Global increase in major tropical cyclone exceedance probability over the past four decades. Proceedings of the National Academy of Sciences 117, 11975–11980.

Kourafalou, V.H., Kang, H., 2012. Florida Current meandering and evolution of cyclonic eddies along the Florida Keys Reef Tract: Are they interconnected? Journal of Geophysical Research: Oceans 117.

Kundu, P.K., 1976. Ekman veering observed near the ocean bottom. Journal of Physical Oceanography 6, 238–242.

Landsea, C.W., Franklin, J.L., 2013. Atlantic hurricane database uncertainty and presentation of a new database format. Monthly Weather Review 141, 3576–3592.

Lane, E.M., Restrepo, J., McWilliams, J.C., 2007. Wave–current interaction: A comparison of radiation-stress and vortex-force representations. Journal of physical oceanography 37, 1122–1141.

Langmuir, I., 1938. Surface motion of water induced by wind. Science 87, 119–123.

Le, H.A., Lambrechts, J., Ortleb, S., Gratiot, N., Deleersnijder, E., Soares-Frazão, S., 2020. An implicit wetting–drying algorithm for the discontinuous galerkin method: application to the tonle sap, mekong river basin. Environmental Fluid Mechanics , 1–29.

Le Hénaff, M., Kourafalou, V.H., Paris, C.B., Helgers, J., Aman, Z.M., Hogan, P.J., Srinivasan, A., 2012. Surface evolution of the Deepwater Horizon oil spill patch: Combined effects of circulation and wind-induced drift. Environmental Science & Technology 46, 7267–7273.

Lee, T.N., Leaman, K., Williams, E., Berger, T., Atkinson, L., 1995. Florida Current meanders and gyre formation in the southern Straits of Florida. Journal of Geophysical Research: Oceans 100, 8607–8620.

Lee, T.N., Mayer, D.A., 1977. Low-frequency current variability and spin-off eddies along the shelf off southeast Florida. Collected Reprints 1, 344.

Lee, T.N., Smith, N., 2002. Volume transport variability through the Florida Keys tidal channels. Continental Shelf Research 22, 1361–1377.

Lee, T.N., Williams, E., 1988. Wind-forced transport fluctuations of the Florida Current. Journal of Physical Oceanography 18, 937–946.

Li, Z., Johns, B., 1998. A three-dimensional numerical model of surface waves in the surf zone and longshore current generation over a plane beach. Estuarine, Coastal and Shelf Science 47, 395–413.

Lin, N., Chavas, D., 2012. On hurricane parametric wind and applications in storm surge modeling. Journal of Geophysical Research: Atmospheres 117.

Liu, Y., Weisberg, R.H., 2012. Seasonal variability on the West Florida shelf. Progress in Oceanography 104, 80–98.

Liu, Y., Weisberg, R.H., Zheng, L., 2020. Impacts of hurricane Irma on the circulation and transport in Florida Bay and the Charlotte Harbor estuary. Estuaries and Coasts 43, 1194–1216.

Liubartseva, S., Coppini, G., Lecci, R., Clementi, E., 2018. Tracking plastics in the Mediterranean: 2D Lagrangian model. Marine Pollution Bulletin 129, 151–162.

Longuet-Higgins, M.S., 1970. Longshore currents generated by obliquely incident sea waves. Journal of geophysical research 75, 6778–6789.

Longuet-Higgins, M.S., Stewart, R., 1964. Radiation stresses in water waves; a physical discussion, with applications, in: Deep sea research and oceanographic abstracts, Elsevier. pp. 529–562.

Madsen, O.S., Poon, Y.K., Graber, H.C., 1989. Spectral wave attenuation by bottom friction: Theory, in: Coastal Engineering 1988, pp. 492–504.

Malmstadt, J., Scheitlin, K., Elsner, J., 2009. Florida hurricanes and damage costs. Southeastern Geographer 49, 108–131.

McWilliams, J.C., Restrepo, J.M., Lane, E.M., 2004. An asymptotic theory for the interaction of waves and currents in coastal waters. Journal of Fluid Mechanics 511, 135.

McWilliams, J.C., Sullivan, P.P., 2000. Vertical mixing by Langmuir circulations. Spill Science & Technology Bulletin 6, 225–237.

Mei, C.C., 1989. The applied dynamics of ocean surface waves. volume 1. World scientific.

Moon, I.J., Ginis, I., Hara, T., Thomas, B., 2007. A physics-based parameterization of air–sea momentum flux at high wind speeds and its impact on hurricane intensity predictions. Monthly Weather Review 135, 2869–2878.

Pinelli, J.P., Roueche, D., Kijewski-Correa, T., Plaz, F., Prevatt, D., Zisis, I., Elawady, A., Haan, F., Pei, S., Gurley, K., et al., 2018. Overview of damage observed in regional construction during the passage of Hurricane Irma over the State of Florida, in: Forensic Engineering 2018: Forging Forensic Frontiers. American Society of Civil Engineers Reston, VA, pp. 1028–1038.

Powell, M.D., Houston, S.H., Amat, L.R., Morisseau-Leroy, N., 1998. The HRD real-time hurricane wind analysis system. Journal of Wind Engineering and Industrial Aerodynamics 77, 53–64.

Powell, M.D., Vickery, P.J., Reinhold, T.A., 2003. Reduced drag coefficient for high wind speeds in tropical cyclones. Nature 422, 279–283.

Röhrs, J., Christensen, K.H., Hole, L.R., Broström, G., Drivdal, M., Sundby, S., 2012. Observation-based evaluation of surface wave effects on currents and trajectory forecasts. Ocean Dynamics 62, 1519–1533.

Schott, F.A., Lee, T.N., Zantopp, R., 1988. Variability of structure and transport of the Florida Current in the period range of days to seasonal. Journal of Physical Oceanography 18, 1209–1230.

Siadatmousavi, S.M., Jose, F., Stone, G., 2011. Evaluation of two WAM white capping parameterizations using parallel unstructured SWAN with application to the Northern Gulf of Mexico, USA. Applied Ocean Research 33, 23–30.

Sikirić, M.D., Roland, A., Janeković, I., Tomazić, I., Kuzmić, M., 2013. Coupling of the Regional Ocean Modeling System (ROMS) and Wind Wave Model. Ocean Modelling 72, 59–73.

Smith, N.P., 1982. Response of Florida Atlantic shelf waters to hurricane David. Journal of Geophysical Research: Oceans 87, 2007–2016.

Stokes, G.G., 1880. On the theory of oscillatory waves. Transactions of the Cambridge Philosophical Society .

Tolman, H.L., et al., 2009. User manual and system documentation of WAVEWATCH III TM version 3.14. Technical note, MMAB Contribution 276, 220.

Van Den Bremer, T., Breivik, Ø., 2018. Stokes drift. Philosophical Transactions of the Royal Society A: Mathematical, Physical and Engineering Sciences 376, 20170104.

Villas Bôas, A.B., Cornuelle, B.D., Mazloff, M.R., Gille, S.T., Ardhuin, F., 2020. Wave–current interactions at meso-and submesoscales: Insights from idealized numerical simulations. Journal of Physical Oceanography 50, 3483–3500.

Wachnicka, A., Browder, J., Jackson, T., Louda, W., Kelble, C., Abdelrahman, O., Stabenau, E., Avila, C., 2019. Hurricane Irmas impact on water quality and phytoplankton communities in Biscayne Bay (Florida, USA). Estuaries and Coasts , 1–18.

Weisberg, R., Liu, Y., Mayer, D., 2009. Mean circulation on the west Florida continental shelf observed with long-term moorings. Geophys. Res. Lett 36, L19610.

Weisberg, R.H., Zheng, L., 2006. Hurricane storm surge simulations for Tampa Bay. Estuaries and Coasts 29, 899–913.

Wu, L., Chen, C., Guo, P., Shi, M., Qi, J., Ge, J., 2011. A FVCOM-based unstructured grid wave, current, sediment transport model, I. Model description and validation. Journal of Ocean University of China 10, 1–8.

Xian, S., Feng, K., Lin, N., Marsooli, R., Chavas, D., Chen, J., Hatzikyriakou, A., 2018. Brief communication: Rapid assessment of damaged residential buildings in the Florida Keys after Hurricane Irma. Natural Hazards and Earth System Sciences 18, 2041–2045.

Zedler, S., Niiler, P., Stammer, D., Terrill, E., Morzel, J., 2009. Ocean's response to Hurricane Frances and its implications for drag coefficient parameterization at high wind speeds. Journal of Geophysical Research: Oceans 114.

Zhang, C., Durgan, S.D., Lagomasino, D., 2019. Modeling risk of mangroves to tropical cyclones: A case study of Hurricane Irma. Estuarine, Coastal and Shelf Science 224, 108–116.